Supplementary Information

Mixed spinel $Ni_{0.5}Zn_{0.5}Fe_2O_4$ on nickel foam for electrocatalytic oxygen evolution reaction: revealing the influence of temperature and promoting performance with zero voltage switching inductive heating

Yujie Guo,[a] Feng Duan,[b] Gaili Ke,[a] Yiming Zhang, [a] Tao Han, [a] Hanmei Jiang, [a] Wenrong Wang, [a] Yong Zhou [c] and Huichao He[a]*

[a]*College of Materials and New Energy, Chongqing University of Science and Technology, Chongqing 401331, China.*

[b]*College of Chemical Engineering, Sichuan University, Chengdu 610064, China.*

[c]*Ecomaterials and Renewable Energy Research Center, School of Physics, University Nanjing, Nanjing 211102, China*

***Corresponding Author'**

Email: hehuichao@cqust.edu.cn (Huichao He)

Table of Content

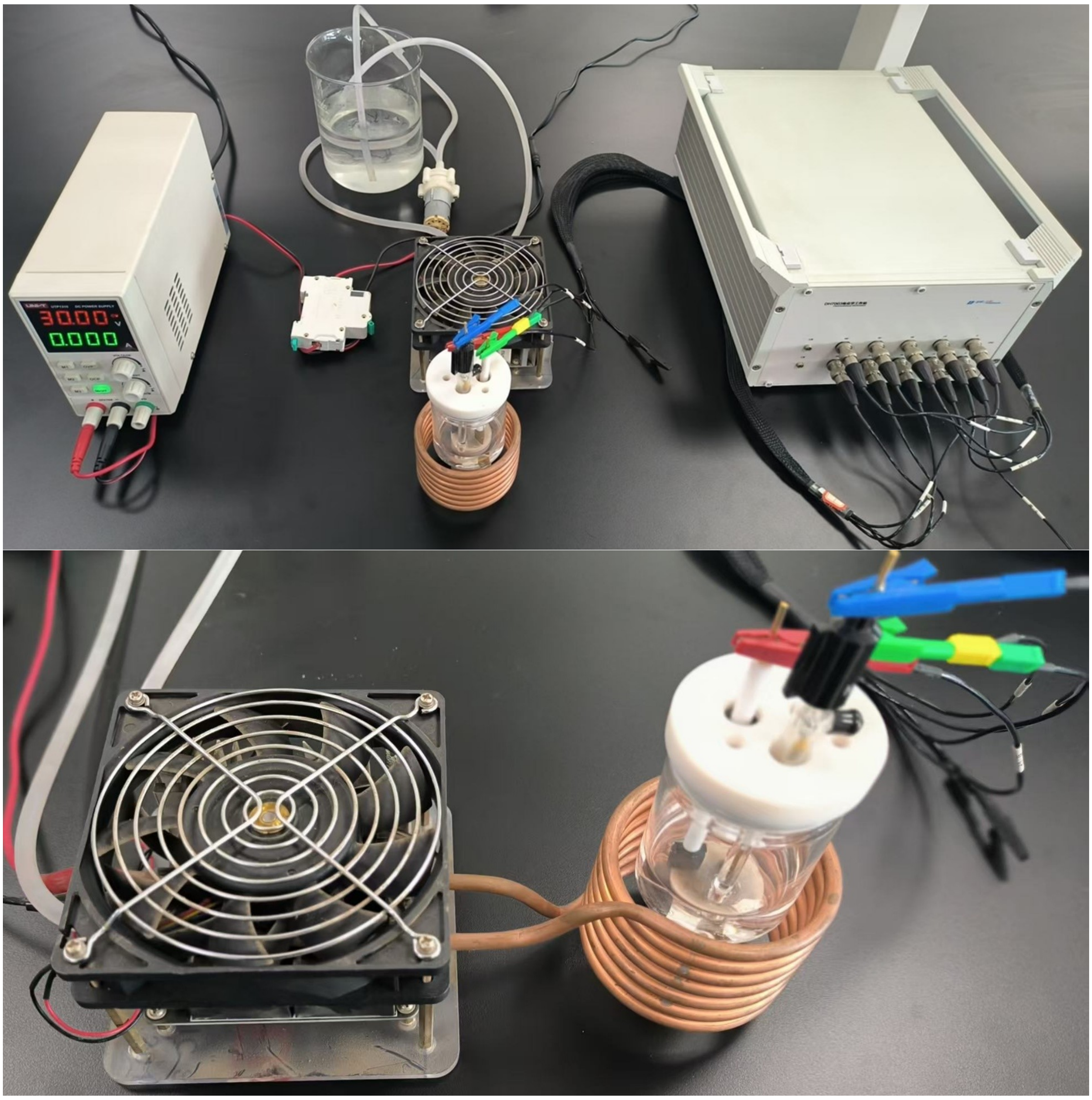

Fig. S1 The photograph of $Ni_{0.5}Zn_{0.5}Fe_2O_4$/NF cell with ZVS induction heater for electrochemical measurements. The ZVS inductive heater was composed of a DC power supply and a ZVS inductive device that was purchased from Shenzhen Huali Electronic Technology *Co.,* Ltd, China.

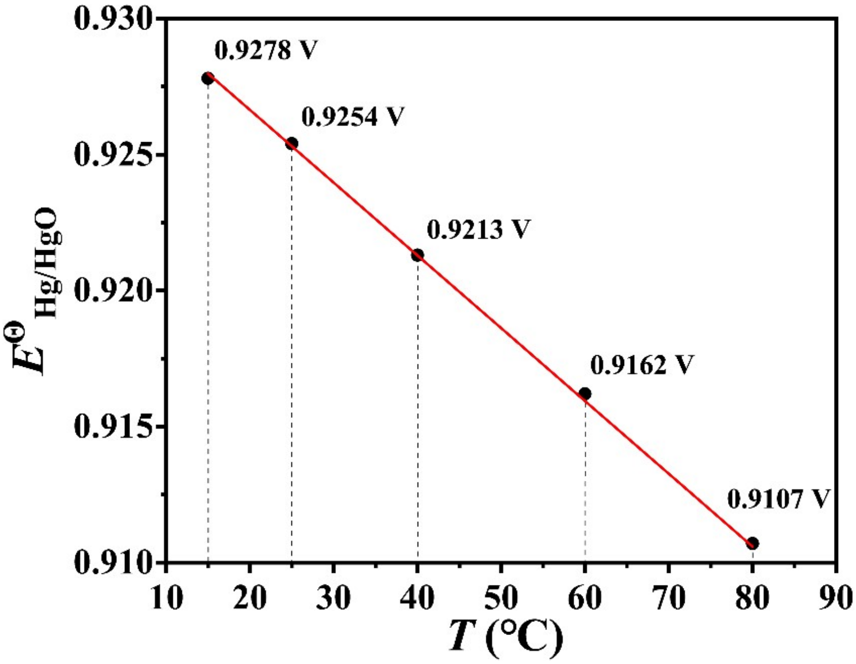

Fig. S2 The standard potential of Hg/HgO reference electrode ($E^{\theta}_{Hg/HgO}$) at different temperatures.

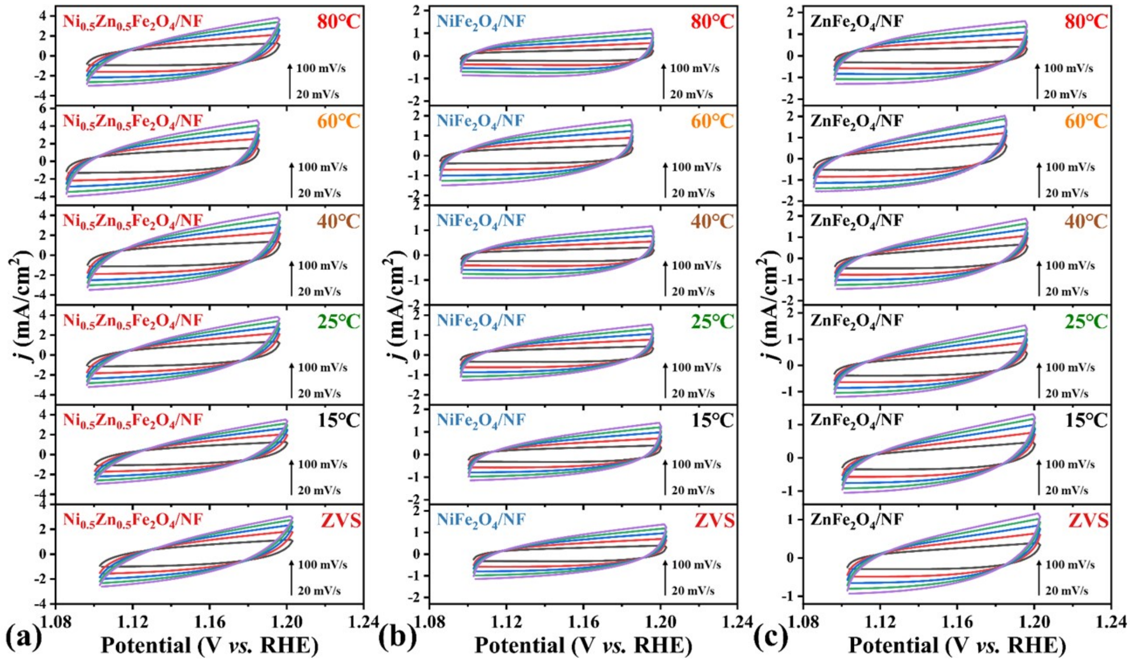

Fig. S3 CV data of $Ni_{0.5}Zn_{0.5}Fe_2O_4$/NF, $NiFe_2O_4$/NF and $ZnFe_2O_4$/NF for their ECSA calculation.

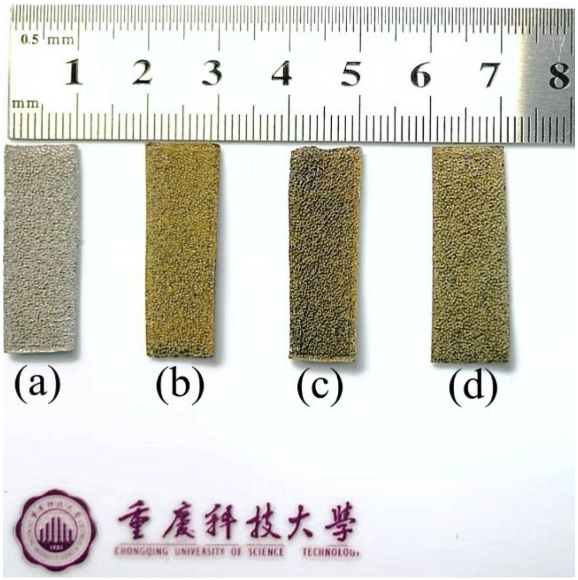

Fig. S4 The photographs of (a) Ni foam, (b) $Ni_{0.5}Zn_{0.5}Fe_2O_4$/NF, (c) $NiFe_2O_4$/NF and (d) $ZnFe_2O_4$/NF sample.

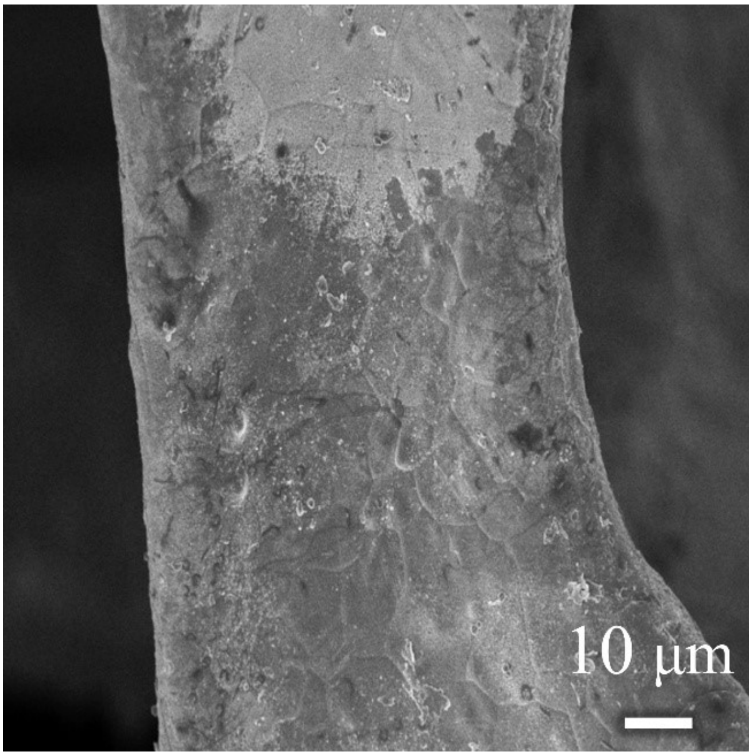

Fig. S5 Low-magnification SEM image of $Ni_{0.5}Zn_{0.5}Fe_2O_4$/NF.

Fig. S6 Raman spectra of $Ni_{0.5}Zn_{0.5}Fe_2O_4$, $ZnFe_2O_4$ and $NiFe_2O_4$ powders.

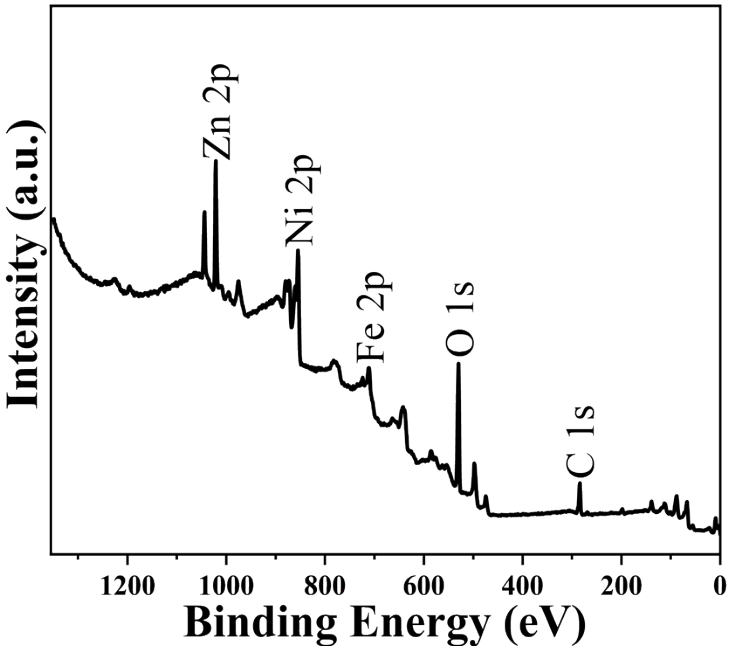

Fig. S7 Survey XPS spectrum of $Ni_{0.5}Zn_{0.5}Fe_2O_4$/NF.

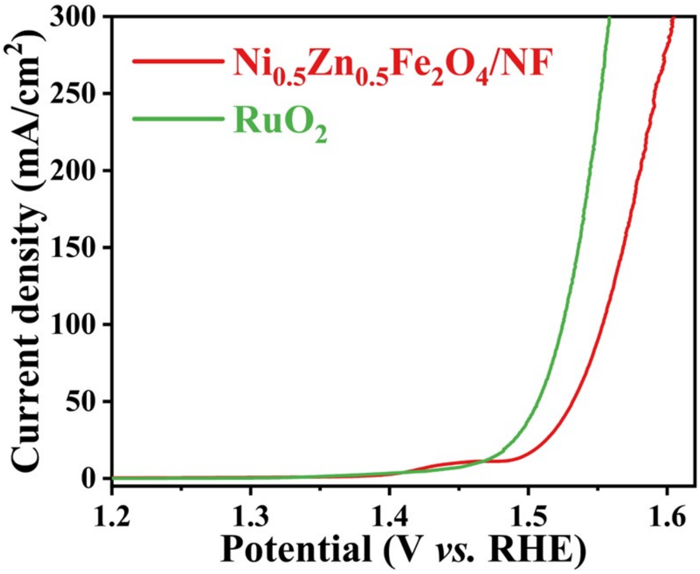

Fig. S8 LSV curves of $Ni_{0.5}Zn_{0.5}Fe_2O_4$/NF and commercial RuO_2 in 25℃ 1.0 M KOH.

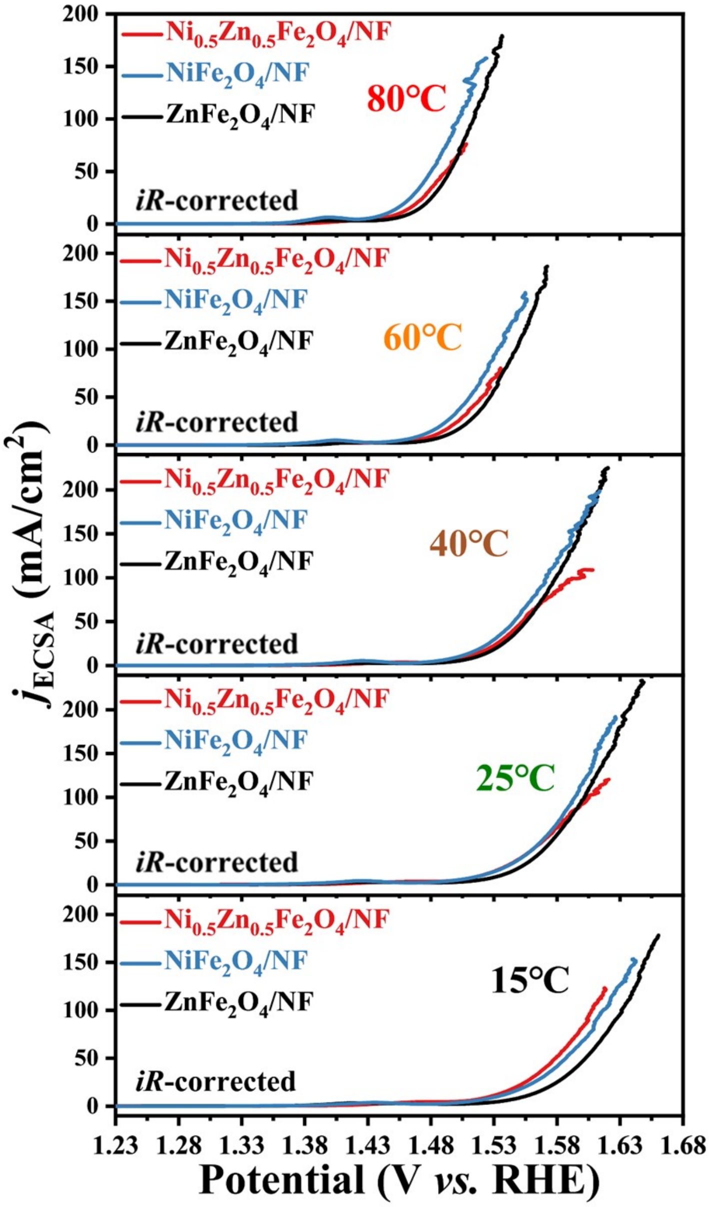

Fig. S9 ESCA-normalized current density (j_{ECSA}) curves of $Ni_{0.5}Zn_{0.5}Fe_2O_4$/NF, $NiFe_2O_4$/NF and $ZnFe_2O_4$/NF in 1.0 M KOH at different temperatures.

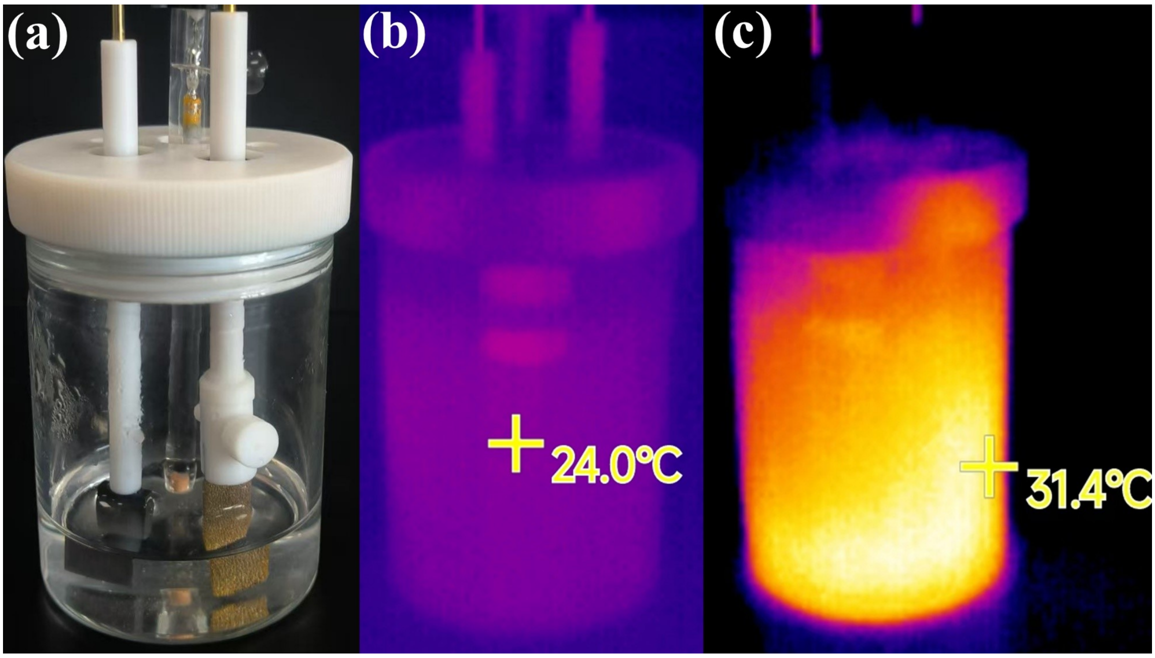

Fig. S10 (a) Photographs of $Ni_{0.5}Zn_{0.5}Fe_2O_4$/NF-based cell for water electrolysis, thermal image of $Ni_{0.5}Zn_{0.5}Fe_2O_4$/NF-based cell (b) before and (c) after ZVS induction heating.

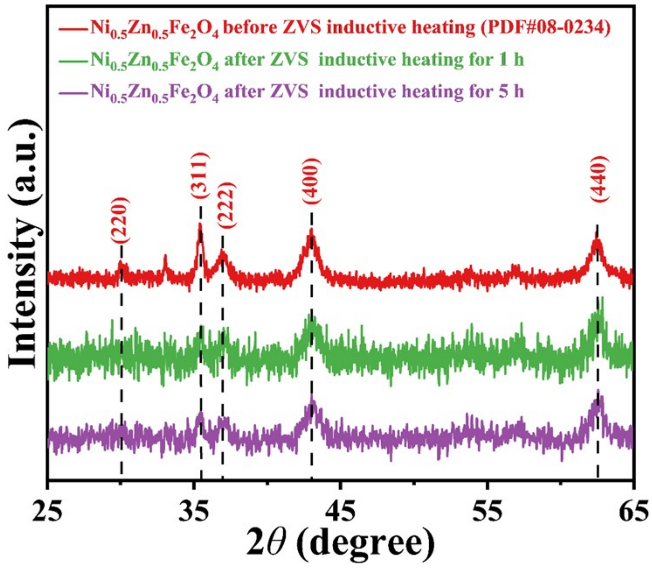

Fig. S11 XRD patterns of $Ni_{0.5}Zn_{0.5}Fe_2O_4$ powders that collected from $Ni_{0.5}Zn_{0.5}Fe_2O_4$/NF before and after ZVS inductive heating for 1h and 5 h.

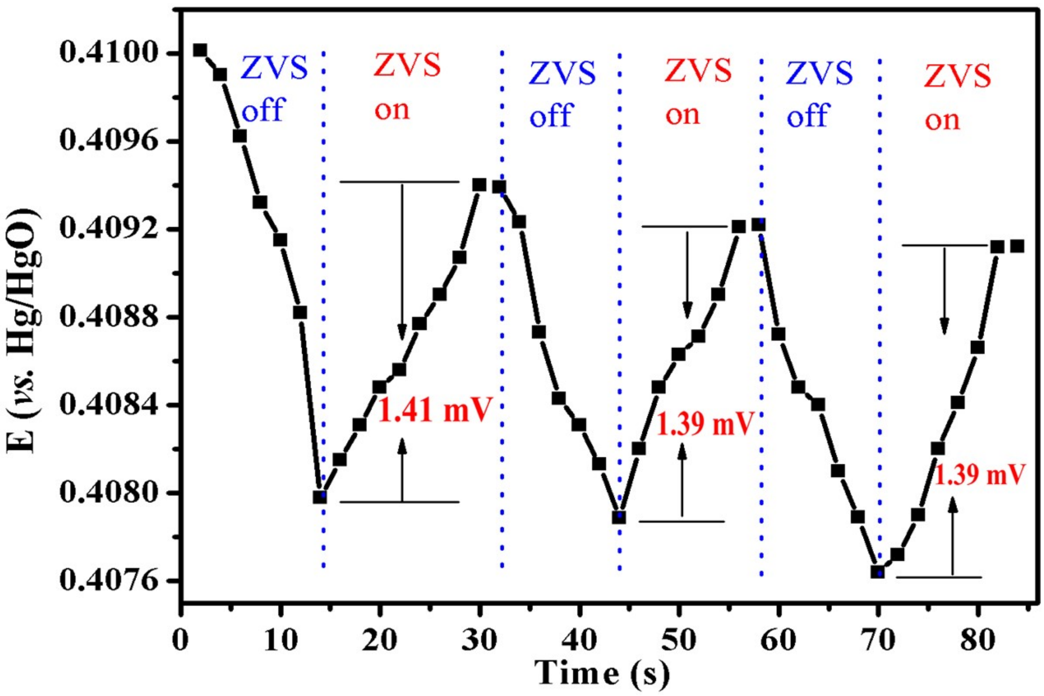

Fig. S12 OCP curve of $Ni_{0.5}Zn_{0.5}Fe_2O_4$/NF in 1.0 M KOH with ZVS inductive heating on and off.

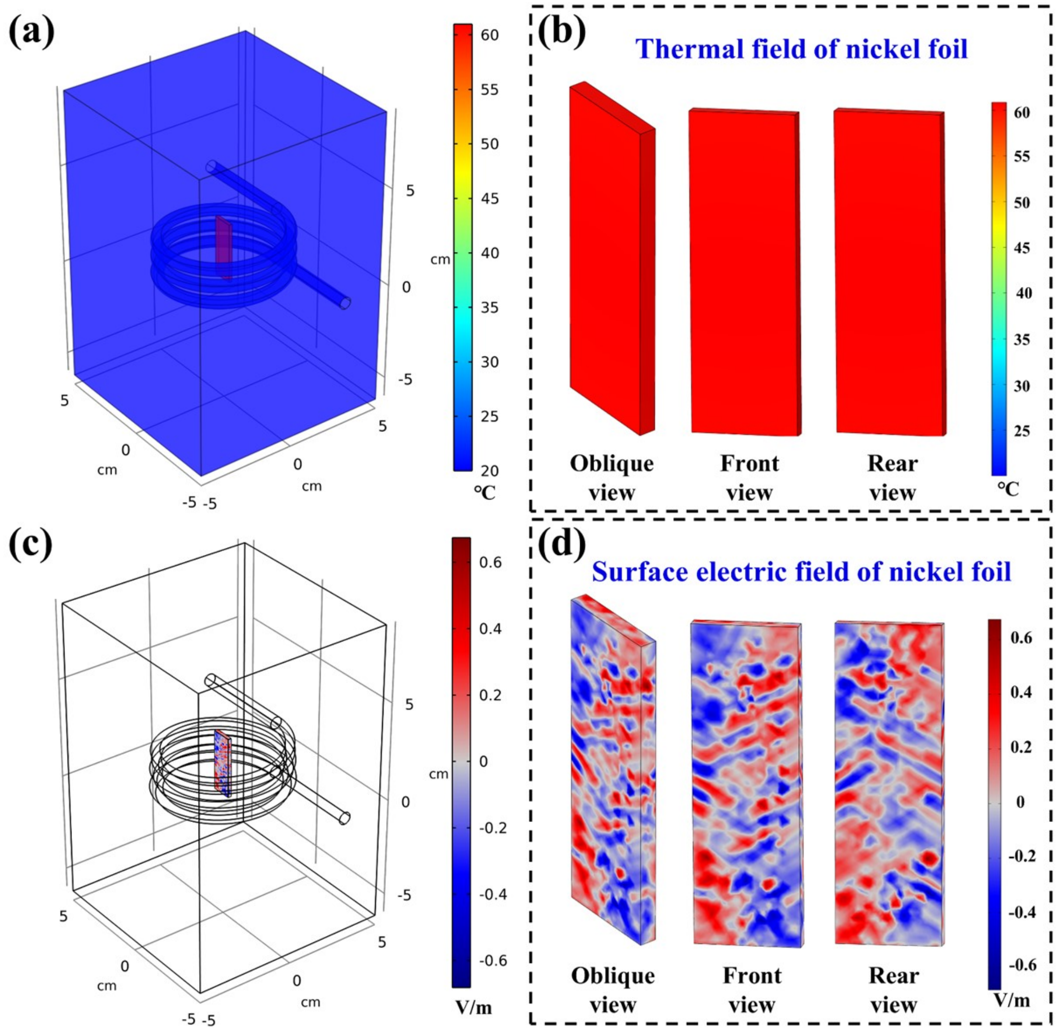

Fig. S13 COMSOL Multiphysics software simulation for the formation of (a, b) thermal field, (c, d) electric field on nickel foil under ZVS inductive heating.

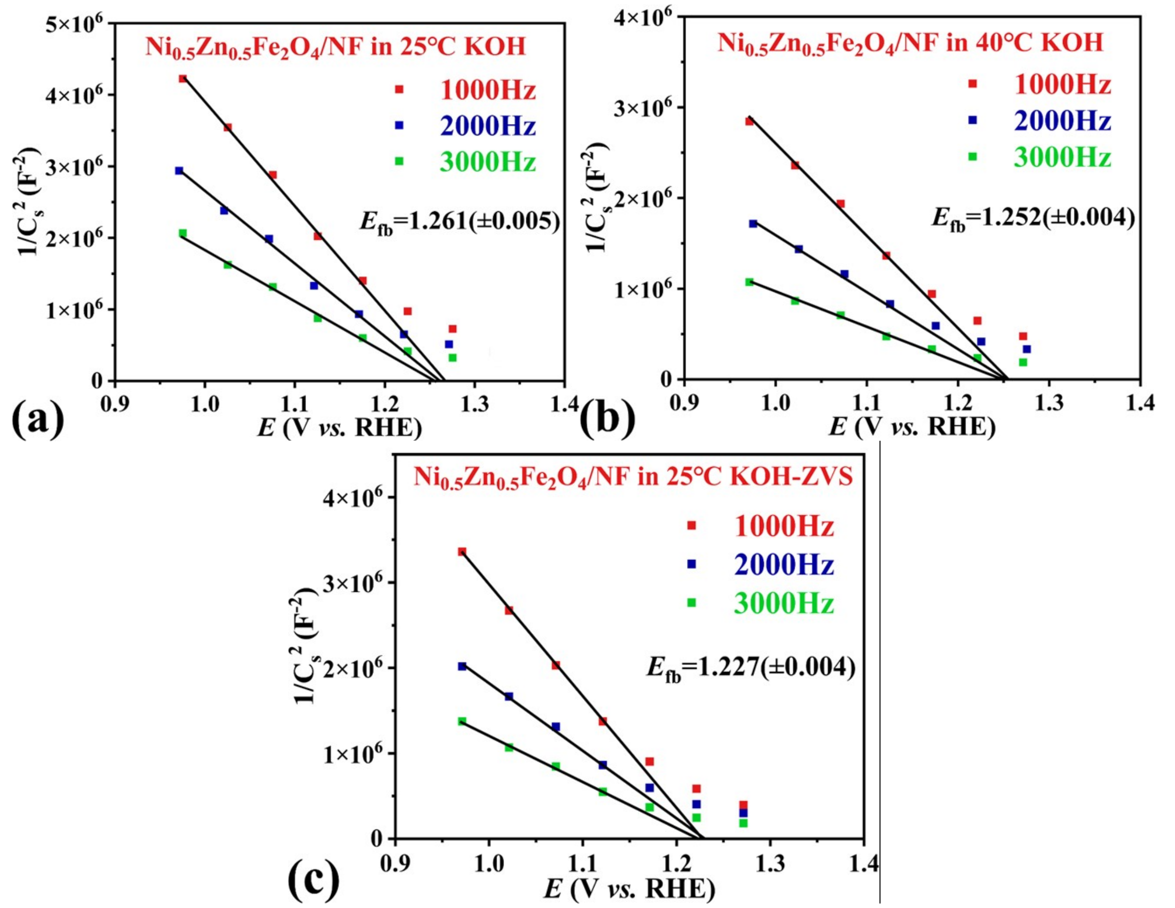

Fig. S14 Mott-Schottky plots of $Ni_{0.5}Zn_{0.5}Fe_2O_4$/NF in (a) 25℃ and (b) 40℃ 1.0 M KOH without ZVS inductive heating, and in (c) 25℃ 1.0 M KOH with ZVS inductive heating.

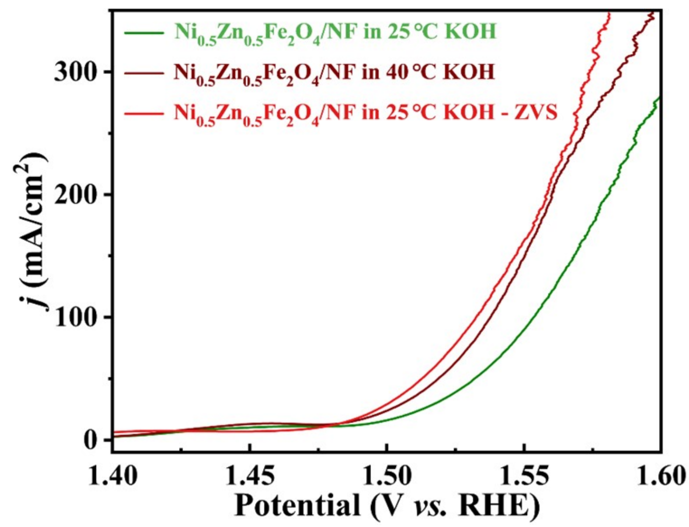

Fig. S15 LSV curve of $Ni_{0.5}Zn_{0.5}Fe_2O_4$/NF in 25℃ and 40℃ 1.0 M KOH without ZVS inductive heating, and in 25℃ under ZVS inductive heating.

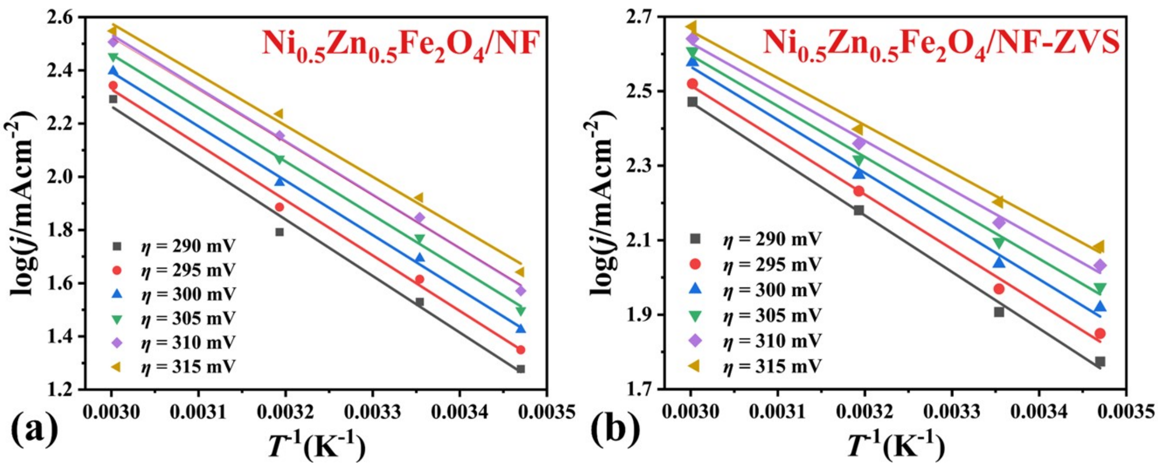

Fig. S16 $\log j$-T^{-1} curves of $Ni_{0.5}Zn_{0.5}Fe_2O_4$/NF in OER Tafel range with and without ZVS inductive heating.

Table S1 The linearity (R^2) of anodic-cathodic current density (ΔI) and the scan rate (v) for ECSA measurements.

Sample \ R^2	15℃	25℃	40℃	60℃	80℃	ZVS
$Ni_{0.5}Zn_{0.5}Fe_2O_4$/NF	0.97	0.97	0.98	0.98	0.98	0.97
$NiFe_2O_4$/NF	0.98	0.98	0.98	0.99	0.98	0.99
$ZnFe_2O_4$/NF	0.98	0.97	0.98	0.99	0.98	0.99

Table S2 OER activity comparison of the resultant $Ni_{0.5}Zn_{0.5}Fe_2O_4$/NF to the previously reported spinel ferrite electrocatalysts.

Electrocatalyst	Overpotential	Reference
$Ni_{0.5}Zn_{0.5}Fe_2O_4$/NF	276 mV@20 mA cm^{-2} 293 mV@36 mA cm^{-2}	This work
$Co_{1.2}Fe_{1.8}O_4$	320 mV10 mA cm^{-2}	1
ZCF-50($Cu_{0.5}ZnFe_2O_4$)	280 mV@10 mA cm^{-2}	2
$NiDy_{0.05}Fe_{1.95}O_4$	360 mV@36 mA cm^{-2}	3
$NiCo_{0.03}Fe_{1.97}O_4$	450 mV@10 mA cm^{-2}	4
$Co_{0.8}Mn_{0.2}Gd_{0.1}Fe_{1.9}O_4$	342 mV@10 mA cm^{-2}	5
$(Mn_{0.2}Co_{0.2}Ni_{0.2}Cu_{0.2}Fe_{0.2})Fe_2O_4$	295 mV@10 mA cm^{-2}	6
$ZnFe_2O_4$	330 mV@10 mA cm^{-2}	7
$Co_{2.25}Fe_{0.75}O_4$	350 mV@10 mA cm^{-2}	8
$(CoNiCuZnMg)Fe_2O_4$	420 mV@10 mA cm^{-2}	9
$NiFe_2O_4$	278 mV@10 mA cm^{-2}	10
$CoFe_2O_4$	350 mV@10 mA cm^{-2}	11
P-Mo-Co_3O_4@CC	276 mV@10 mA cm^{-2}	12
SFO/Sm-NFO	228 mV@10 mA cm^{-2}	13
Ta-NiFe LDH	260 mV@50 mA cm^{-2}	14
$CoNiFeO_x$-NC	265 mV@50 mA cm^{-2}	15

References

(1) Fabiano R. Praxedes *et al.* Synergetic Phenomenon between Structural Distortion and Cobalt Valence State and its Effect on the Oxygen Evolution Reaction in Cobalt Ferrites. *Ceramics International.* 2025, DOi.org/10.1016/j.ceramint.2025.06.010.

(2) Navid Attarzadeh *et al.* Enhanced Electrocatalytic Activity of Ecofriendly and Earth-Abundant (Zn,Cu)Fe_2O_4+CuO Nanocomposites for Water Splitting. *ACS Applied Materials & Interfaces.* 2025, 17(19), 28038-28054.

(3) A.R. Panda *et al.* Multifunctionality exploration of dysprosium-doped $NiFe_2O_4$: An efficient bifunctional electrocatalyst toward ORR/OER, *Journal of Rare Earths.* 2025, Doi.org/10.1016/j.jre.2025.03.023.

(4) Sonnu Benny *et al.* Engineering of cobalt impregnated sponge like spinel nickel ferrite as an efficient electrocatalyst for sustained overall water splitting. *Inorganic Chemistry Communications*. 2025, 174(2), 114044.

(5) Prachi Jain *et al.* Production of cost-effective green energy using Mn/Gd co-substituted cobalt ferrites hydroelectric cells and their oxygen evolution reaction. *Journal of Alloys and Compounds*. 2025, 1010,177419.

(6) Radhamadhab Das *et al.* High-Entropy Spinel Oxide: A Prolific System of Panoramic Functional Properties. *Journal of Physical Chemistry C*. 2024 128 (34), 14168-14184.

(7) Nyemaga M. Malima *et al.* Solvent-Less Synthesis of Compositionally Tuned Mixed Metal (Ni−Zn) Ferrites for Enhanced Electrocatalytic Water Splitting and Supercapacitance. *ChemElectroChem.* 2024, 11, e202400181.

(8) Sascha Saddeler *et al.* Influence of the cobalt content in cobalt iron oxides on the electrocatalytic OER activity. *Journal of Materials Chemistry A*. 2021, 9, 25381-25390.

(9) Marcus Einert *et al.* Sol-Gel-Derived Ordered Mesoporous High Entropy Spinel Ferrites and Assessment of Their Photoelectrochemical and Electrocatalytic Water Splitting Performance. *Small.* 2023, 19, 2205412.

(10) Laura A. Achola *et al.* Microwave Hydrothermal Synthesis of Mesoporous First-Row Transition Metal Ferrites. *Chemistry of Materials.* 2022, 34(17), 7692–7704.

(11) Ping Guo *et al.* Unveiling the Coercivity-Induced Electrocatalytic Oxygen Evolution Activity of Single-Domain $CoFe_2O_4$ Nanocrystals under a Magnetic Field. *The Journal of Physical Chemistry Letters.* 2022, 13(32), 7476–7482.

(12) Yujie Huang *et al.* Plasma-induced Mo-doped Co_3O_4 with enriched oxygen vacancies for electrocatalytic oxygen evolution in water splitting. *Carbon Energy.* 2022, 5(3), e279.

(13) Juhyung Choi *et al.* Tuning the electronic structure and inverse degree of inverse

spinel ferrites by integrating samarium orthoferrite for efficient water oxidation. *Applied Catalysis B: Environmental.* 2022, 315, 121504.
(14) Xueyuan Wang *et al.* Ta-doping triggered electronic structural engineering and strain effect in NiFe LDH for enhanced water oxidation. *Chemical Engineering Journal.* 2021, 403, 126297.
(15) Chen, Chen *et al.* Hierarchical trimetallic Co-Ni-Fe oxides derived from core-shell structured metal-organic frameworks for highly efficient oxygen evolution reaction. *Applied Catalysis B: Environmental.* 2021, 287, 119953.